Periodic Dispersion-Corrected Approach for Isolation Spectroscopy of N_2 in an Argon Environment: Clusters, Surfaces and Matrices

Y. Makina, [a)] K. Mahjoubi,[a)] D. M. Benoit, [b),*] N.-E. Jaidane,[a)] M. Mogren Al-Mogren,[c)] and M. Hochlaf [d),*]

[a)] Laboratoire de Spectroscopie Atomique, Moléculaire et Applications – LSAMA, Université de Tunis El Manar, Tunis, Tunisie.

[b)] Department of Chemistry, University of Hull, HU6 7RX, UK.

[c)] Chemistry Department, Faculty of Science, King Saud University, PO Box 2455, Riyadh 11451, Kingdom of Saudi Arabia

[d)] Université Paris-Est, Laboratoire Modélisation et Simulation Multi Echelle, MSME UMR 8208 CNRS, 5 bd Descartes, 77454 Marne-la-Vallée, France

*) Corresponding authors:

D. M. Benoit: D.Benoit@hull.ac.uk

M. Hochlaf: hochlaf@univ-mlv.fr

ABSTRACT

ab initio and PBE density functional theory with dispersion correction (PBE-D3) calculations are performed to study N_2–Ar_n ($n \leq 3$) complexes and N_2 trapped in Ar matrix (*i.e.* N_2@Ar). For cluster computations, we used both Møller-Plesset (MP2) and PBE-D3 methods. For N_2@Ar, we used a periodic-dispersion corrected model for Ar matrix, which consists on a slab of four layers of Ar atoms. We determined the equilibrium structures and binding energies of N_2 interacting with these entities. We also deduced the N_2 vibrational frequency shifts caused by clustering or embedding compared to an isolated N_2 molecule. Upon complexation or embedding, the vibrational frequency of N_2 is slightly shifted whilst its equilibrium distance remains unchanged. This is due to the weak interactions between N_2 and Ar within these compounds. Our calculations show the importance of inclusion of dispersion effects for the accurate description of geometrical and spectroscopic parameters of N_2 either isolated, in interaction with Ar surfaces or trapped in Ar matrices.

I. INTRODUCTION

The study of interactions between rare-gas atoms and molecules provides a wealth of information on molecular properties (matrix spectroscopies, for example) but also on how their properties are modified by their environments (i.e. matrix shift) [1]. It has been shown that if the interaction between the rare-gas atoms and the molecule is weak, the molecular properties are only slightly perturbed by the surrounding environment and thus are a very close to those of the isolated molecule [2]. This condition is satisfied for neutral van der Waals (vdW) complexes containing molecules interacting with rare gas atoms [3]. Such interactions play important roles in several chemical, physical and biological media [3-8]. They are in subtle balance with electrostatic (ES) and exchange-repulsion (ER) interactions. For instance, they control the 3D structures of DNA and proteins, crystal packing, aggregates formation, and the orientation of molecules when approaching surfaces [9,10].

Several theoretical and experimental studies have been devoted to probing the spectroscopy of di- and poly-atomic molecules interacting with either rare-gas atoms or rare-gas matrices. These include, for instance, CO, NO, Cl_2, CO_2, C_3, O_3 and NO_2 molecules [4-8] interacting with Ne, Ar, Kr or Xe. A full understanding of the effects occurring at the atomic scale requires reliable and relevant information on the potential energy surfaces of these systems. However, obtaining reliable interaction potentials remains challenging due to the many-body nature of those systems.

High accuracy wave-function methods such as the coupled-cluster methods (for example CCSD(T) at the complete basis set (CBS) limit) provide an excellent account of the dispersion energy. However, these methods still suffer from unfavorable computational scaling [$O(N^7)$] leading to large computation times even for medium-sized systems. Density functional theory (DFT), on the other hand, has an intrinsically lower computational cost, but standard approaches do not describe dispersion interactions accurately. To try to correct this drawback, various DFT techniques have been proposed to improve the description of dispersion interactions in the theory. Those are, for example, the non-local van der Waals density functional (vdW-DF) [11,12], the DFT symmetry-adapted perturbation theory (DFT-SAPT) [13,14] including more rigorous partitioning of intermolecular energies, the density functional theory/coupled cluster method (DFT/CC) based on the pairwise representability of the difference between the CCSD(T) and DFT energies [15], the density functional (DF) that takes into account the dispersion interaction from a physical point of view [16], and the empirically-corrected DFT-D approach [17-20]. Over the years, the DFT-D approach has been widely used because of its simplicity, low computational overhead and reliability.

The present contribution examines the case of an N_2 molecule interacting with small Ar clusters, surfaces or embedded into an Ar matrix. Because of its importance for atmospheric and planetary processes [21,22], the Ar–N_2 cluster has been widely studied both theoretically [23-35] and experimentally [36-39]. These studies have provided an accurate characterization of this complex, of its potential energy surface and of its vibrational and rotational spectra. In particular, they established

the existence of two minima of Ar–N_2: a linear structure and a T-shaped structure, located in shallow potential wells (a few tens of cm^{-1}). Note that large and medium-sized mixed Ar_n-N_{2m} clusters (n > 200) have also been widely investigated [40-46] whereas we are not aware of studies of small N_2–Ar_n clusters ($1 \leq n \leq 5$). In the case of methane clusters, for example, Sanaa Zaag et al. [47] showed that small clusters may behave differently and possess different properties and reactivities than medium-sized or large clusters. Hence small N_2–Ar_n clusters deserve specific investigations, which is one of the aims of this study.

The present computations were carried out using the same first–principles methodology for all environments (gas phase clusters, molecules adsorbed on a rare-gas surface or embedded into a rare-gas matrix). We compute the equilibrium structures and interaction potentials thus enabling us to examine the vibrational and structural effects caused by clustering or embedding. This highlights the induced environment effects on the structure and the spectroscopy of N_2. Moreover, we establish the efficiency of the DFT-D3 method in accounting for the anisotropy of the interaction at the molecular level for all types of environments studied.

Our paper is arranged as follows: we briefly describe the computational details in Section II. Our results for N_2–Ar_n clusters are presented in Section III. Section IV contains the data relative to N_2 adsorbed on Ar surfaces or embedded in an Ar matrix. We discuss our findings in Section V.

II. COMPUTATIONAL METHODS

The DFT-D approach considers dispersion as an additive, pairwise, energy correction term, C_6R^{-6}, where R and C_6 are the interatomic distances and the dispersion coefficients, respectively [19,48,49]. Various versions of DFT-D have been proposed. The latest iteration proposed by Grimme *et al.* [13,18] includes third-order dispersion corrections and removes some of the initial empiricism (DFT-D3). Moreover, Grimme and co-workers introduced geometry-dependent information to improve transferability that was lacking in DFT-D1 [19] and DFT-D2 [20]. Several benchmark studies showed that DFT-D3 results differ from those obtained with CCSD(T) by less than 5-10% [17,18,50,51]. In addition, this approach has been shown to provide a reliable description of rare-gas interactions, which are usually hard to describe using uncorrected DFT functionals [52].

In this study, we use the Gaussian plane waves (GPW) method [53-57] to account for the periodicity of the embedded system. This approach uses pseudopotential associated Gaussian basis sets for the expansion of the Kohn–Sham valence orbitals, and auxiliary plane waves basis set for the description of the electronic density as implemented in the Quickstep code [56,58,59], which is a part of the CP2K open source program [60]. The interaction of valence electrons with the nuclei is modeled by means of relativistic, norm-conserving, separable, dual-space Gaussian-type pseudopotentials of Goedecker, Teter, and Hutter (GTH) [61], optimized for the gradient-corrected exchange-correlation functional of Perdew, Burke, and Ernzerhof (PBE) [62]. This functional is used for all our calculations following a careful benchmarking in our previous study [52].

For molecular systems, a cut-off energy E_{cut} = 400 Ry was found to be sufficient. The atomic geometry of the matrix models, surfaces, molecules and dimers are optimized by minimizing the energy using the BFGS optimizer [63]. The convergence criteria between the current and the last optimizer iteration are: the maximum geometry change is set to 5×10^{-4} bohr, the root mean square (RMS) geometry change is set to 2.5×10^{-4} bohr and the maximum force component of the current configuration is set to 10^{-6} bohr^{-1} × Hartree.

To model the N_2–Ar_n cluster systems, we use a supercell of 20 × 20 × 20 Å in size. We remove the periodic images and use a 0-D analytic Poisson solver for the electrostatic terms. We use the QZV3P-GTH basis set [53,64] for Ar atoms and the diffuse aug-QZV3P-GTH basis set [53,64] for N atoms (the exponents of all polarization functions are taken from Dunning's aug-cc-pVXZ (X = T, Q) basis sets [16,65]). The N_2-Ar_n (n = 1, 2, 3) clusters are computed using Moller-Plesset second-order perturbation theory (MP2) [65–67] in conjunction with Dunning and co-worker's aug-cc-pVXZ (X= T, Q) basis sets as implemented in Gaussian 09 package [68]. Additional CCSD(T) calculations are performed using the CFOUR suite of programs (V1.0) [69].

For each system, the DFT-D3 total energy is computed as the sum of the conventional DFT energy and the correction value based on a damped atom-pairwise potential [17]. The counterpoise correction for the basis set superposition error (BSSE) [70] was not considered during the DFT-D3 calculation for our large systems (adsorbed molecule and embedded into Ar matrices), as suggested by Grimme [17,18] but was used for all wave-function based cluster calculations.

III. N_2–Ar_n (n = 0, 1, 2, 3) CLUSTERS

a) The Isolated Nitrogen Molecule

We start our investigations by a series of test calculations for the isolated N_2 molecule to benchmark our theoretical approach, the basis sets and the pseudopotentials. We compute the equilibrium distance and the vibrational frequency of isolated N_2 in its electronic ground state ($X^1\Sigma_g^+$) using CCSD(T) and MP2 post Hartree–Fock methods in conjunction with the aug-cc-pVXZ (X= T, Q) basis sets. We also use the dispersion-corrected Density Functional Theory using the PBE functional with the GTH pseudopotential and aug-TZV2P or aug-QZV3P basis sets. Our results and their comparison to experimental data are listed in Table 1.

Table 1: Equilibrium Distance (r_e, Å) and Harmonic Vibrational Frequency (ω_e, cm^{-1}) of N_2 ($X^1\Sigma_g^+$) Computed Using Various Methods and Basis Sets. The Notation FC Indicates Frozen-Core CCSD(T) Calculations. Deviations From the Experimental Results are Given in Square Brackets. Note that the Given Experimental Vibrational Frequency is the Harmonic Value. The Experimental Fundamental Frequency for N_2 is $\tilde{\nu} = 2329.9\ cm^{-1}$ [71].

Method	Basis set	r_e	ω_e
MP2	aug-cc-pVTZ	1.114 [0.016]	2186.8 [–171.8]
	aug-cc-pVQZ	1.110 [0.012]	2201.6 [–157.0]
PBE-D3	aug-TZV2P-GTH	1.102 [0.004]	2350.9 [–7.7]
	aug-QZV3P-GTH	1.102 [0.004]	2344.8 [–13.8]
CCSD(T)	aug-cc-pVTZ(FC)	1.104 [0.006]	2340.0 [–18.6]
	aug-cc-pVQZ(FC)	1.101 [0.003]	2354.5 [–4.1]
Experiment [a)]	---	1.098	2358.6

a) Ref. [71].

Table 1 shows that MP2 provides the least satisfactory description of both distances and frequencies, with deviations of the order of ~0.01 Å and ~171 cm^{-1}, respectively. As expected, CCSD(T) leads to an order of magnitude improvement for both quantities, with largest deviations of the order of ~0.006 Å and ~20 cm^{-1} and will be considered as computational reference for our study. Interestingly, both PBE-D3/aug-TZV2P and PBE-D3/aug-QZV3P-GTH give the same distance (1.102 Å) which is similar to that obtained with CCSD(T). For the harmonic vibrational frequency, MP2/aug-cc-pVXZ (X= T, Q) levels underestimate ω_e in comparison to experiment (deviations of more than 170 cm^{-1}) whereas CCSD(T) and PBE-D3 reassuringly agree well with the experimental value (differences of few cm^{-1} for the largest basis sets). The correlation effects present in the N–N system are poorly described by MP2, which is to be expected. However, PBE-D3 combined with either aug-TZV2P-GTH or aug-QZV3P-GTH basis sets performs as well as CCSD(T)/aug-cc-VQZ. This is particularly interesting given the much lower computational cost of PBE-D3 as compared to CCSD(T). Therefore, PBE-D3/aug-QZV3P-GTH constitutes a cost-effective method of choice for the description of N_2 in various environments.

b) The N_2–Ar Cluster

The N_2–Ar complex is a typical system that displays van der Waals interactions. It is characterized by the dominance of pure dispersion interactions. As mentioned in the introduction, two minimum energy structures exist for the N_2–Ar cluster: a T-shaped form and a linear form. The geometrical parameters and harmonic vibrational frequencies of these two stable geometries are listed in Table 2.

Table 2: Harmonic Frequencies (ω_i, cm^{-1}) and Equilibrium Geometries of T-shaped and Linear Structures of N_2–Ar Complex. r_e, R and θ are the Jacobi Coordinates (Figure 1). Distances are in Å and Angles are in Degrees. ω_1 is the Harmonic Vibrational Frequency of N_2. The Vibrational Shift From the Free N_2 Frequency is Shown in square Brackets. BE (meV) is the Binding Energy of the Complex.

Linear form			
Method	MP2 [a)]	PBE-D3 [b)]	CCSD(T) [c)]
r_e	1.11	1.10	1.10
R	4.72	4.37	4.20
θ	0.0	0.0	0.0
BE	–8.9	–13.4	–9.7 (Ref [14])
ω_1	2185.4 [+1.4]	2344.9 [–0.2]	2339.3 [+0.7]
ω_2	36.9	217.4	35.1
ω_3	6.0	191.1	12.6
T-shaped form			
Method	MP2 [a)]	PBE-D3 [b)]	CCSD(T) [c)]
r_e	1.11	1.10	1.10
R	3.63	3.75	3.68
θ	90.0	89.8	90.0
BE	–11.2	–17.3	–12.4 (Ref [14])
ω_1	2185.3 [+1.5]	2344.9 [–0.2]	2339.5 [–0.5]
ω_2	41.4	231.7	36.4
ω_3	12.3	177.0	6.1

a) aug-cc-pVTZ basis set

b) aug-QZV3P-GTH and QZV3P-GTH basis sets for N and Ar.

c) aug-cc-pVTZ basis set.

Table 2 shows that our computed equilibrium parameters R and θ (as defined in Figure 1 below) are in satisfactory agreement with the high-level CCSD(T) calculations. Indeed, the R distance is 4.37 Å for PBE-D3 and 4.20 Å at the CCSD(T) level for the linear form of N_2–Ar and R = 3.75 Å and R = 3.68 Å using PBE-D3 and CCSD(T) for the T-shaped form, whereas MP2 provides an R distance that deviates noticeably from CCSD(T) for the linear form. As was the case above for isolated N_2, MP2 underestimates the N–N stretch, while PBE-D3 is remarkably close to CCSD(T). Overall, the magnitude of the vibrational shift is small (~1.5 cm^{-1} for MP2, ~0 cm^{-1} for PBE-D3 and ~0.5 cm^{-1} for CCSD(T)) and remains similar for both configurations at all levels of theory.

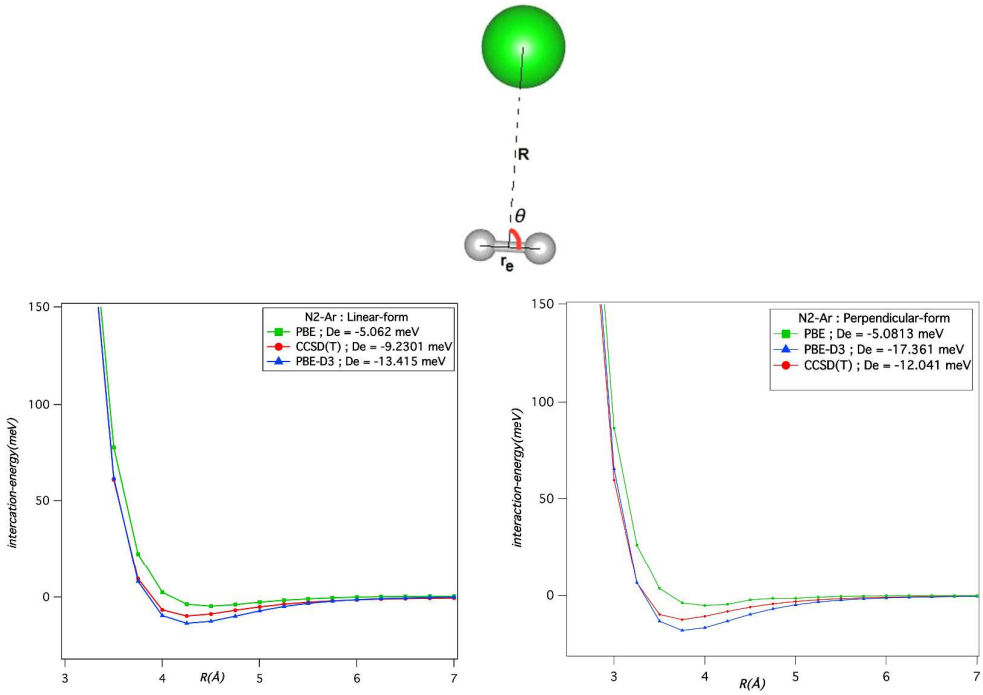

Figure 1: Upper panel: Definition of the r_e, R and θ parameters. Lower panel: Potential energy for T-shaped and linear forms of N_2–Ar obtained with PBE DFT with and without dispersion correction D3, where Ar is described using the QZV3P basis set and N by the aug-QZV3P-GTH basis set. We also show the potential calculated at the CCSD(T)/aug-cc-pVTZ+BF level [24].

Figure 1 displays one-dimensional cuts of the 3D potential energy surface (3D-PES) of N_2–Ar along the R Jacobi coordinate for perpendicular (θ = 90°, T-shape form) and collinear (θ = 0°, linear form) configuration. These potentials are computed using the PBE-D3 method with and without dispersion correction (i.e. standard PBE) and compared to the CCSD(T) calculations of Ref [24]. This enables us to assess the performance of the corrected dispersion density functional method for this van der Waals complex. For these cuts, the N–N distance (r_e) is fixed at 1.10 Å.

Figure 1 shows that PBE, PBE-D3 and CCSD(T) potentials present minima, corresponding to the T-shaped and linear N_2–Ar clusters. Nevertheless, the depth of these potential wells depends on the method used for computations. Indeed, we compute a binding energy (BE) of the T-shaped form of –5.1 meV, –17.3 meV and –12.0 meV using PBE, PBE-D3 and CCSD(T), respectively. For the linear form, BE is evaluated –5.1 meV, –13.4 meV, –9.2 meV at the PBE, PBE-D3 and CCSD(T) levels. Our results indicate clearly that including the dispersion correction D3 is crucial for the description of the potential energy with DFT since it leads to deeper potentials, in agreement with the CCSD(T) results. Hence, D3 dispersion correction improves the characterization of the energy profile of these vdW systems. Nevertheless, it seems that PBE-D3 overestimates the dispersion energy as the well depths

are overestimated for both forms. Our results on this cluster indicate clearly that we can use a dispersion-corrected density functional level of theory to compute weak non-bonded interactions.

c) The N_2–Ar_2 System

For the N_2–Ar_2 complex, we limited our geometry optimizations to the global minimum which corresponds to a structure where both argon atoms are close to each other. This structure is displayed in Figure 2 and described in Table 3, with a summary of its geometrical parameters and harmonic vibrational frequencies. Note that the minimum energy structure is similar to the most stable form of the CO–Ar_2 system (denoted as Minimum 1 in Ref. [52]).

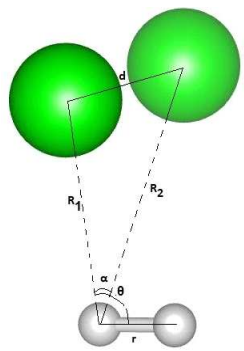

Figure 2: The optimized structure of N_2–Ar_2 system. We give also the definition of the geometrical parameters listed in Table 3.

The binding energy of the complex (BE) is computed as the energy difference between the cluster and that of a free N_2 molecule and an Ar_2 dimer. Using MP2, the BE is computed to be –26.7 meV which is smaller than the value obtained using PBE-D3 (–33.5 meV).

Table 3: Harmonic Frequencies (ω_i, cm^{-1}) and Geometrical Parameters of the N_2–Ar_2 Structure at Equilibrium Computed Using MP2/aug-cc-pVTZ and PBE-D3/aug-TZV2P (N)/QZV3P (Ar) Methods. Distances are in Å and Angles are in degrees. ω_1 is the Harmonic Vibrational Frequency of N_2. The Vibrational Shift From the Free N_2 Frequency is Shown in Square Brackets. BE (meV) is the Binding Energy of the Complex Computed as the Energy Difference Between the Cluster and that of a Free N_2 Molecule and an Ar_2 Dimer.

Parameters	MP2	PBE-D3
r	1.11	1.10
R_1	3.65	3.86
R_2	3.65	3.86
D	3.76	3.81

θ	79.8	80.0
α	61.9	61.0
ω_1	2183.8 [+3]	2343.5 [+1.3]
ω_2	47.7	205.1
ω_3	35.8	203.0
ω_4	29.9	186.1
ω_5	13.5	142.0
ω_6	11.3	29.0
BE	–26.7	–33.5

Table 3 also shows that the N–N distance remains almost unchanged upon clustering whereas the harmonic vibrational frequency of N_2 decreases by 1.3 cm^{-1} using PBE-D3 method (but by 3 cm^{-1} at MP2 level) with respect to that of isolated N_2 molecule. Therefore, there is a negligible effect of complexation on the N-N distance, whereas the N_2 harmonic vibrational frequency is affected. We note that, compared to the CO–Ar_2 complex [52], the inter-monomer distances (R_1, R_2) are longer for N_2–Ar_2. This is due to the slightly weaker interaction between N_2 and Ar_2 as compared to that of CO and Ar since N_2 is non-polar.

d) The N_2–Ar_3 System

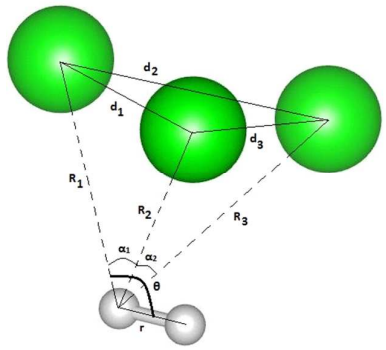

Figure 3: Optimized structure of N_2–Ar_3 system and definition of the parameters listed in Table 4.

Figure 3 presents the most stable form of the N_2–Ar_3 cluster, which is obtained after several geometry optimizations with different starting structures. This stable structure is formed by a quasi-equilateral triangle constructed by the three Ar atoms situated above the N_2 molecule. The binding energy of this cluster, computed as the energy difference between the cluster and that of a free N_2

molecule and that of an Ar_3 trimer, is –39.6 meV at the MP2 level and –46.2 meV using the PBE-D3 approach.

Table 4: Harmonic Frequencies (ω_i, cm^{-1}) and Geometrical Parameters of N_2–Ar_3 Structure Using MP2/aug-cc-pVTZ and PBE-D3/aug-TZV2P (N)/QZV3P (Ar) Methods. Distances are in Å and Angles in degrees. ω_1 is the Harmonic Vibrational Frequency of N_2. The Vibrational Shift From the Free N_2 Frequency is Shown in Square Brackets. BE (meV) is the Binding Energy of the Cluster, Computed as the Energy Difference Between the Cluster and that of a Free N_2 Molecule and that of an Ar_3 Trimer.

Parameters	MP2	PBE-D3
R	1.114	1.102
R_1	3.523	3.725
R_2	4.137	4.285
R_3	3.523	3.725
d_1	3.748	3.930
d_2	3.759	3.987
d_3	3.748	3.924
θ	99.36	99.73
α_1	57.92	58.2
α_2	57.91	58.4
ω_1	2182.1 [+4.7]	2342.9 [+1.9]
ω_2	54.0	208.0
ω_3	51.1	204.9
ω_4	40.3	195.1
ω_5	37.6	148.3
ω_6	27.7	142.5
ω_7	27.7	34.7
ω_8	13.2	24.6
ω_9	8.1	22.8
BE	–39.6	–46.2

Table 4 summarizes the geometrical parameters of this structure. The Ar–N_1–Ar angles (α_i) are similar for both methods, 58°, but there is a difference in the Ar_1–N_1–N_2 angle (θ) as seen previously for the N_2–Ar_2 complex. Also, we notice that the distance between the two nitrogen atoms remains

almost unchanged within N_2–Ar_3 as compared to that of isolated N_2. As noticed above for N_2–Ar_2, the distances between Ar and N atoms are longer than those computed for CO–Ar_3 [52] because of the weaker dispersive interaction between N_2 and Ar. Note that the computed harmonic vibrational frequency shift for N_2 is more noticeable, amounting to ~2 cm^{-1} using the PBE-D3 method (4.7 cm^{-1} at MP2 level). This is an increase in magnitude compared to N_2–Ar_2. Note also that the harmonic vibrational frequency of N_2 is smaller than that of isolated N_2 ($X^1\Sigma_g^+$).

IV. N_2 Interacting with Ar Surfaces or Trapped in Ar Matrices

In the previous section, we showed that the PBE-D3/aug-QZV3P level of theory gives accurate enough results, which agree well with CCSD(T) or experimental values for the isolated and clustered nitrogen molecule. This is associated with a significant reduction of the computational cost compared to CCSD(T), for example. Thus larger systems, such as N_2 adsorbed on Ar surfaces or trapped in Ar cold matrices, can be explored with similar accuracy using this approach.

a) Pure Ar Crystal

We choose to study four layers of 18 Ar atoms as a periodic model for the Ar matrix, which leads to a cubic unit cell containing 72 Ar atoms. After a PBE-D3/QZV3P optimization of our model crystal, we calculate a face centered cubic (fcc) lattice of 5.223 Å. This value agrees well with the experimental value (of 5.222 Å) measured at 0 K by Fujii et al. [72] and with the theoretical value (of 5.30 Å) by Migen Halo *et al.* [73] derived using periodic MP2 computations.

b) N_2 Interacting with an Ar Surface

For these computations, we used our four argon layers model and added ~20 Å of vacuum above the surface to construct the super-lattice. The N_2 molecule is then positioned above the Ar surface. The large size of our super-cell (15.669 ×15.669 ×25 Å) minimizes any N_2–N_2 neighboring periodic interaction. We performed three sets of calculations. We started by fixing all argon atoms, then, we released the Ar planes one by one by moving away from the molecule. The model where all Ar layers are fully frozen is denoted as "All 4 layers". When only the first Ar layer (first two Ar layers) is relaxed the model is denoted as "Bottom 3 layers" (as "Bottom 2 layers"). Two starting orientations of the nitrogen molecule were chosen: either perpendicular or parallel to the surface. The results of these computations are collected in Table 5, where we list the N–N equilibrium distance, its harmonic frequency and the vibrational shift caused by surface attachment. We also give the binding energy (BE) of N_2 to the surface computed as the energy difference between the system and that of a free N_2 molecule and the relaxed argon surface.

After optimization, two stable configurations were found: N_2 parallel to the surface and N_2 perpendicular to the surface. Since the electron density on both N atoms is the same, the tilt angle (δ) of the molecular axis of the N_2 molecule with respect to the Ar surface is 0° or 90°. Note that for

anisotropic electron densities, δ is different from these two values. This is the case, for instance, for CO adsorbed on Ar surface [52], or for imidazole and histidine interacting with a gold Au (111) surface [74,75].

Table 5: Characteristics of the Interaction of N_2 Located Parallel or Perpendicular to an Argon Surface. r_e (Å) and ω_e (cm^{-1}) are the N-N Equilibrium Distance and the N_2 Harmonic Vibrational Frequency, respectively. $\Delta\omega_e$ (cm^{-1}) corresponds to the Vibrational Shift with respect to Free N_2. R_e (Å) is the Distance from the Centre of Mass of N_2 and the First Ar Layer. BE (meV) is the Binding Energy Surface Computed as the Energy Difference Between the System and that of a Free N_2 Molecule and the Relaxed Argon Surface.

Number of frozen Ar layers	r_e	ω_e	$\Delta\omega_e$	R_e	BE
N_2 // Ar_{72}					
All 4 layers	1.10	2335.3	+9.5	3.74	–42.9
Bottom 3 layers	1.10	2335.0	+9.8	3.71	–45.0
Bottom 2 layers	1.10	2335.0	+9.8	3.79	–45.2
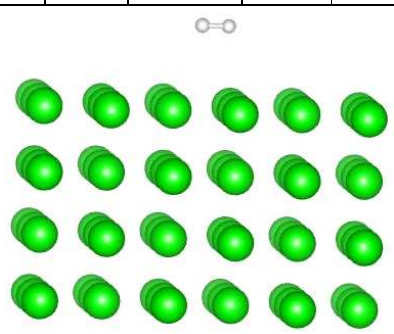					
$N_2 \perp Ar_{72}$					
All 4 layers	1.10	2357.2	–12.4	3.69	–25.4
Bottom 3 layers	1.10	2356.9	–12.1	3.66	–28.3
Bottom 2 layers	1.10	2357.3	–12.5	4.02	–28.8
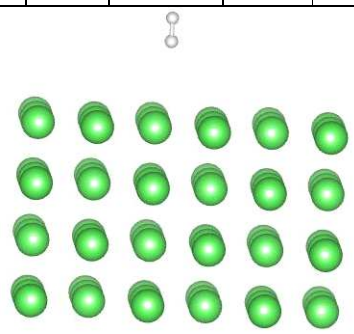					

Table 5 lists the equilibrium geometries of N_2 interacting with the Ar surface models. This table shows that the N−N equilibrium distance remains unchanged regardless of the orientation of the nitrogen molecule on the argon surface. The distance between N_2 and the Ar surface (R_e ~3.4 Å) is relatively long. The computed harmonic frequencies of N_2 are 2335 cm^{-1} and 2357 cm^{-1} for N_2 // Ar_{72} and $N_2 \perp Ar_{72}$ respectively, which correspond to approximate vibrational shifts of +10 cm^{-1} and –12 cm^{-1} compared to isolated N_2, respectively. Interestingly, relaxing the Ar layers does not influence the adsorption geometry which is different to what was observed for CO interacting with Ar surface [52]. Yet the binding energies of N_2 to the surface differ and BE is –45.2 meV for N_2 // Ar_{72} and –28.8 meV for $N_2 \perp Ar_{72}$. This is consistent with what was observed earlier for the two minimum energy structures of N_2–Ar (linear and T-shaped) with unchanged N–N distance, but different BEs (stronger binding for the T-shaped structure). Thus, the perpendicular orientation of N_2 on the Ar surface is similar to the linear stationary point of N_2–Ar and the parallel orientation of N_2 on the Ar surface is similar to the T-shaped stationary point of N_2–Ar. This is also in agreement with the data obtained for N_2–Ar_2 and N_2–Ar_3. The vibrational shift is strongly dependent on the binding mode with a positive shift for the parallel arrangement and a negative shift for the perpendicular arrangement.

c) N_2 Molecule Trapped in Argon Matrices

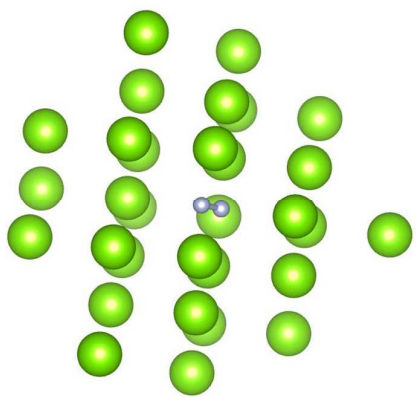

N_2–Ar_{31}

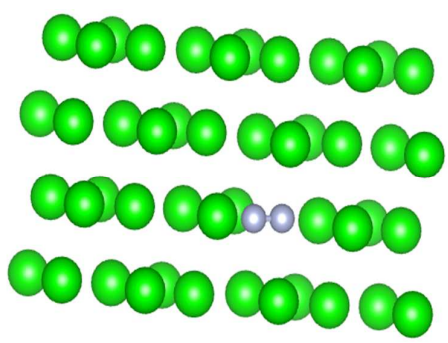

N_2–Ar_{47}

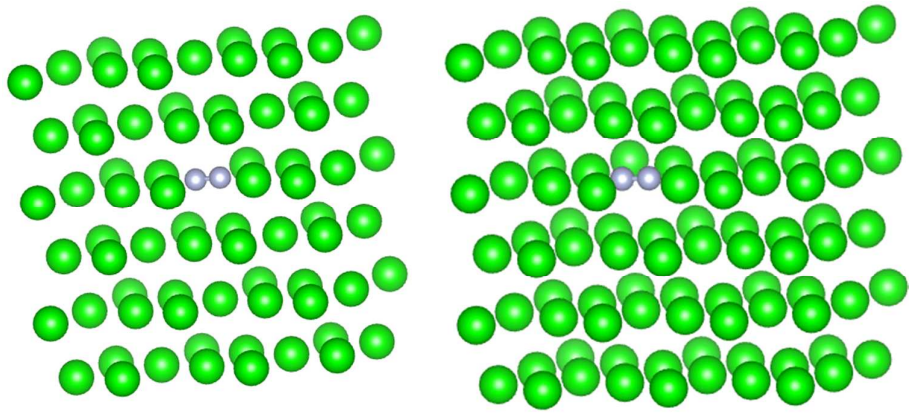

N_2–Ar_{74} **N_2–Ar_{107}**

Figure 4: Optimized equilibrium structures of N_2 embedded in argon matrices of different sizes.

We treated the nitrogen molecule trapped in argon matrix using PBE-D3 in order to evaluate the effect of the gas rare environment around this diatomic. For that purpose, we used the optimum geometry calculated for pure Ar crystal and we replaced one Ar atom situated in the centre of the unit cell by a N_2 molecule. This procedure ensures that the N_2 molecule is fully embedded in a periodic argon environment. Moreover, we have used four unit cells obtained by translation of the primary unit cell, cell size effects of (2x2x2), (3x2x2), (3x3x2) and (3x3x3) were used to assess these effects. These correspond to N_2–Ar_{32}, N_2–Ar_{47}, N_2–Ar_{74} and N_2–Ar_{107}, where the separation between adjacent nitrogen diatomics increases with the number of Ar atoms in the matrix. Then we performed geometry optimizations. The parameters of the equilibrium structures are depicted in Figure 4 and reported in Table 6.

The experimental vibrational shift is inherently anharmonic as it is computed using the difference between the measured fundamentals for N_2@Ar (Ref. [76]) and that for a free N_2 molecule (Ref. [71]). In our calculations, we use the computed harmonic frequency of N_2 trapped in argon matrix (Table 6) and the value computed for an isolated N_2 molecule (Table 1) assuming that the anharmonicity constant remains similar in both cases. This approximation allows us to estimate the experimental vibrational shift using only the harmonic approximation.

Table 6: Characteristics of N_2 Embedded into Ar Matrices. r_e (Å) is the Equilibrium Distance of N_2. ω_e (cm^{-1}) is the N_2 Harmonic Vibrational Frequency. $\Delta\omega_e$ (cm^{-1}) Corresponds to the Vibrational Shift with Respect to Free N_2. R_{NAr} (Å) Corresponds to the Distance Between Ar and N and $R_{N2\text{-}N2}$ (Å) is the Distance Between N_2 and its Periodic Image.

System	r_e	ω_e	$\Delta\omega_e$	R_{NAr}	$R_{N2\text{-}N2}$
free N_2	1.103	2344.8	0	–	–
N_2@Ar_{31}	1.102	2367.6	–22.8	3.37	10.6
N_2@Ar_{47}	1.103	2340.8	+4.0	3.42	12.1

N_2@Ar_{74}	1.103	2335.6	+9.2	3.98	14.2
N_2@Ar_{107}	1.103	2335.6	+9.2	3.91	15.5
N_2@Ar_{matrix} a)	–	2325.9	+4.0	–	–

a) Ref. [76].

Upon embedding, the N–N equilibrium distance (r_e) remains almost unchanged. For N_2@Ar_{31}, the N_2 stretch frequency is computed to be 2367 cm^{-1} (negative vibrational shift). However, this shift increases as we increase the size of the matrix. Indeed, Table 6 shows that there is a slight decrease in the N_2 harmonic vibrational frequency from ~2345 cm^{-1} for isolated N_2 to 2340–2335 cm^{-1} for N_2 trapped in a matrix made of 47 or 74 or 107 Ar atoms per unit cell. Convergence is reached with an Ar matrix containing at least 74 Ar atoms. The corresponding harmonic vibrational frequency shifts remain then constant at the value of ~9 cm^{-1}.

Thus, N_2 trapped into a unit cell containing 31 Ar atoms is most likely too small a model to prevent N_2 from interacting with its periodic image. Indeed, the lateral interactions between N_2 and its N_2 image (N_2–N_2) could be the cause for the intermediate harmonic frequency value, as the distance between N_2 and its periodic image is of ~10.6 Å. For cells formed by more than 74 Ar the separation between N_2 and its image is larger than 14.2 Å and the harmonic N_2 frequency starts converging. In fact, both cells of 31 and 47 Ar atoms are insufficient to completely solvate N_2. This contrasts with our previous study of CO [52] where the convergence started already with 31 Ar atoms. Since both diatomics have similar sizes, this difference could be related to the different interactions in the CO@Ar and N_2@Ar systems, as N_2 is non-polar while CO is polar.

The frequency shift of N_2 trapped in an Ar matrix remains invariant and converges when the nitrogen is fully solvated in the argon matrix (Ar_{74} matrix). Our theoretical study gives $\Delta\omega_{N2}$ ~9 cm^{-1} which is in agreement with the experimental shift (~4 cm^{-1} [76]). The remaining deviation can be attributed to anharmonic corrections (which have been assumed to be negligible in this study), possible impurities in the experimental Ar matrix or an overestimation of the weak interactions in the system by the DFT-D3 approach.

V. DISCUSSION

Our systematic study of the interaction of nitrogen molecule with different environments of argon shows that the presence of argon atoms surrounding the N_2 molecule disturbs its vibrational structure. Indeed, the harmonic vibrational frequency of nitrogen decreases linearly as the number of Ar atoms in the clusters increase until it reaches a plateau for a number of Ar atoms larger than 3. The largest deviation upon clustering or embedding with respect to free N_2 is of ~9 cm^{-1}. Indeed, the harmonic vibrational frequency of N_2 is nearly unaffected by the presence of a single argon atom. Once we add another Ar atom (N_2–Ar_2, N_2–Ar_3) the vibrational frequency shift increases to ~2 cm^{-1}. For N_2 interacting with Ar surfaces or embedded in Ar matrices, the shift becomes distinctly larger (~9

cm^{-1}). In addition, we notice that the vibrational shift of N_2 interacting with an Ar surface is subject to strong orientation effects when N_2 is perpendicular to the Ar surface (negative vibrational shift) or parallel to the Ar surface (positive vibrational shift).

For CO–Ar_n [52] and HCl–Ar_n (n = 1, 2, 3), these effects are slightly larger [77]. Indeed, the frequency shifts for CO–Ar_n are in the range ~3 cm^{-1} to ~8 cm^{-1} for $1 \leq n \leq 3$. This shift equals 1.76 cm^{-1} for HCl–Ar then becomes 4.53 cm^{-1} when HCl interacts with three Ar atoms. These differences may be related to the polarity of the embedded molecule. The gas rare effects on the harmonic vibrational frequency are in the following order $\Delta\omega_{N2} < \Delta\omega_{HCl} < \Delta\omega_{CO}$, which is roughly proportional to the polarity of the diatomic interacting with gas rare environment (i.e. $\mu_{N2} = 0$, $\mu_{CO} = 0.11$ D and $\mu_{HCl} = 1.109$, in Debye), although stronger for CO.

VI. CONCLUSIONS

The present work attempts to assess and evaluate the performance of the corrected dispersion density functional method in describing N_2–Ar_n van der Waals complexes, which are characterized by the dominance of pure dispersion interactions. Hence, we show that dispersion-corrected DFT provides an accurate and reliable framework to investigate weak interactions between small molecules and noble gas atoms. We illustrate also the use of the Grimme's PBE-D3 approach which may provide a uniform formalism for the treatment of molecules in gas phase, adsorbed on surfaces or embedded in matrices, and in solid state. Our results reveal that there are slight changes on both geometrical parameters and vibrational frequency on N_2 upon embedding on van der Waals matrices. We also demonstrate that these effects remain unchanged from cluster containing few Ar atoms up to full matrix embedding (up to 107 Ar atoms surrounding N_2). These effects are rationalized in terms of the equivalence of bimolecular interaction potentials between N_2–Ar and Ar–Ar species.

Using a periodic approach to matrix embedding, we show that we can model the N_2 molecule and its interactions with a rare gas matrix. However, cautions should be taken when comparing spectroscopic data obtained using matrix embedding to measurements in the gas-phase or to theoretical data of individual molecules, since the influence on spectroscopic properties can be significant. This approach has been developed in our laboratories to treat embedding of CO molecule and it is currently being further developed for other neutral and charged molecules relevant for astrophysical, planetary or atmospheric media (e.g. CN, N_2^+, CO_2 …).

ACKNOWLEDGMENTS

We acknowledge the International Scientific Partnership Program ISPP at King Saud University for funding this research work through ISPP# 0045 and the Marie Curie International Research Staff Exchange Scheme Fellowship within the 7th European Community Framework Program under Grant No. IRSES- GA-2012-31754. We acknowledge the VIPER high-performance

computing facility of the University of Hull and its support team. The supports of the COST Actions CM1405 (MOLIM: MOLecules In Motion) and CM1401 (Our Astro-Chemical History) are also acknowledged.

References

(1) Sauer, J.; Ugliengo, P.; Garrone, E.; Saunders, V. R. Theoretical Study of van der Waals Complexes at Surface Sites in Comparison with the Experiment. *Chem. Rev.* **1994**, *94*, 2095-2160.

(2) Grimme, S. and Steinmetz, M. Effects of London dispersion correction in density functional theory on the structures of organic molecules in the gas phase. *Phys. Chem. Chem. Phys.* **2013**, *15*, 16031-16042.

(3) Grimme, S. Density functional theory with London dispersion corrections. *Comput. Mol. Sci.* **2011**, *1*, 211–228.

(4) Andrews, L. Spectroscopy of Molecular Ions in Noble Gas Matrices. *Ann. Rev. Phys. Chem.* **1979**, *30*, 79-101.

(5) Chabbi, H.; Dahoo, P. R.; Lakhlifi, A. Spectroscopy of O_3 trapped in rare gas matrices. II. Vibrational energies and transition moments of low-lying levels. *J. Chem. Phys.* **1999**, *111*, 10202-10209.

(6) Cahill, J. E.; Leroi, G. E. Raman Spectra of Solid CO_2, N_2O, N_2, and CO. *J. Chem. Phys.* **1969**, *51*, 1324-1331.

(7) Boursey, E.; Roncin, J. Y. Experimental Deperturbation of the $b^1\Pi_u \leftarrow X^1\Sigma^+_g$ Transition of N_2 in the Solid State, Pure and Trapped in Ne and CF_4 Matrices at Low Temperature. *Phys. Rev. Lett.* **1971**, *26*, 308-311.

(8) Fraenkel, R.; Haas, Y. Trapping of guests in a rare gas matrix: A molecular dynamics simulation. *J. Chem. Phys.* **1994**, *100*, 4324- 4328.

(9) Busseron, E.; Ruff, Y.; Moulin E.; Giuseppone N. Supramolecular self-assemblies as functional nanomaterials. *Nanoscale*. **2013**, *5*, 7098-7140.

(10) Dhotel, A.; Chen, Z.; Delbreilh, L.; Youssef, B.; Saiter, J-M.; Tan, L. Molecular Motions in Functional Self-Assembled Nanostructures. *Int. J. Mol. Sci.* **2013**, *14*, 2303-2333.

(11) Becke, A. D. Density-functional thermochemistry. V. Systematic optimization of exchange-correlation functional. *J. Chem. Phys.* **1997**, *107*, 8554-8560.

(12) Langreth, D. C.; Dion, M.; Rydberg, H.; Schröder, E.; Hyldgaard, P.; Lundqvist, B.I. Van der Waals density functional theory with applications. *Int. J. Quantum Chem.* **2005**, *101*, 599-610.

(13) Jeziorski B.; Szalewicz, K. in: edited by von Rague-Schleyer P. *Encyclopedia of Computational Chemisty*; Wiley, New York, Vol. 2, **1998**, p.1376.

(14) Jansen G.; Heßelmann, A. Comment on "Using Kohn−Sham Orbitals in Symmetry-Adapted Perturbation Theory To Investigate Intermolecular Interactions". *J. Phys. Chem. A.* **2001**, *105*, 11156-11157.

(15) Bludský, O.; Rubeš, M.; Soldán, P.; Nachtigall, P. Investigation of the benzene-dimer potential energy surface: DFT/CCSD(T) correction scheme. *J. Chem. Phys.* **2008**, *128*, 114102.

(16) Dunning Jr., T.H. Gaussian basis sets for use in correlated molecular calculations. I. The atoms boron through neon and hydrogen. *J. Chem. Phys.* **1989**, *90*, 1007-1023.

(17) Grimme, S.; Antony, J.; Ehrlich, S.; Krieg, H. A consistent and accurate ab initio parametrization of density functional dispersion correction (DFT-D) for the 94 elements H-Pu. *J. chem. Phys.* **2010**, *132*, 154104.

(18) Grimme, S.; Hansen, A.; Brandenburg, J. G.; Bannwarth, C. Dispersion-Corrected Mean-Field Electronic Structure Methods. *Chem. Rev.* **2016**, *116*, 5105-5154.

(19) Grimme, S. Accurate description of van der Waals complexes by density functional theory including empirical corrections. *J. Comput. Chem.* **2004**, *25*, 1463-1473.

(20) Grimme, S. Semiempirical GGA-type density functional constructed with a long-range dispersion correction. *J. Comput. Chem.* **2006**, *27*, 1787-1799.

(21) Slanina, Z.; Kim, S. J.; Fox, K. Thermodynamics of Ar-N_2 Complexes and Their Abundance in Titan's Atmosphere. *Thermochimica Acta.* **1994**, *232*, 111-116.

(22) Crifo, J. F.; Slanina, Z.; Vigasin, A. *Molecular Complexes in Earth's Planetary, Cometary and Interstellar Atmospheres*. World Scientific Publishing, Singapore, 1998.

(23) Slanina, Z.; Kim, S. J.; Fox, K. Computational studies of atmospheric chemistry species. Part XI. A computational study of two Ar-N_2 complexes. *J. molec. Struct. Theochem* **1993**, *288*, 17-20.

(24) Zhu, J.; Lu, Y.-P.; Chen, X.-R.; Cheng, Y. Ab initio study for the intermolecular interaction potential surface of Ar-N_2 complex. *Eur. Phys. J. D.* **2005**, *33*, 43-48.

(25) Beneventi, L.; Casavecchia, P.; Volpi, G. G.; Wong, C. C. K.; McCourt, F. R. W. Multiproperty determination of a new N_2–Ar intermolecular interaction potential energy surface. *J. Chem. Phys.* **1993**, *98*, 7926-7939.

(26) Wang, F.; McCourt, F. R. W.; Le Roy, R. J. Use of simulated infrared spectra to test N2–Ar pair potentials and dipole moment surfaces. *Mol. Phys.* **1996**, *88*, 821- 840.

(27) Wishnow, E. H.; Gush, H. P.; Ozier, I. Far-infrared spectrum of N_2 and N_2-noble gas mixtures near 80 K. *J. Chem. Phys.* **1996**, *104*, 3511-3516.

(28) Naumkin, F.Y. Molecular versus atom-atom interaction anisotropy in the case of the Ar-N2 van der Waals system. *Mol. Phys.* **1997**, *90*, 875-888.

(29) Fernandez, B.; Koch, H.; Makarewicz, J. Accurate intermolecular ground state potential of the Ar–N_2 complex. *J. Chem. Phys.* **1999**, *110*, 8525-8532.

(30) Wang, F.; McCourt, F. R. W.; Le Roy. R. Dipole moment surfaces and the mid- and far-IR spectra of N_2Ar. *J. Chem. Phys.* **2000**, *113*, 98-106.

(31) Patel, K.; Butler, P. R.; Ellis, A. M.; Wheeler, M. D. Ab initio study of Rg–N_2 and Rg–C_2 van der Waals complexes (Rg=He, Ne, Ar). *J. Chem. Phys.* **2003**, *119*, 909-920.

(32) Munteanu, C. R.; Cacheiro, J. L.; Fernández, B. Accurate intermolecular ground state potential of the Ar-N_2 van der Waals complex. *J. Chem. Phys.* **2004**, *121*, 10419-10425.

(33) Dham, A. K.; McCourt, F. R. W.; Meath, W. J. Exchange-Coulomb Model Potential Energy Surface for the N_2–Ar Interaction. *J. Chem. Phys.* **1995**, *103*, 8477-8491.

(34) Dham, A. K.; Meath, W. J.; Jechow, J. W.; McCourt, F. R. W. New exchange-Coulomb N2–Ar potential-energy surface and its comparison with other recent N_2–Ar potential-energy surfaces. *J. Chem. Phys.*, **2006**, *124*, 034308-22.

(35) Fu, H.; Zheng R.; Zheng, L. Theoretical studies of three-dimensional potential energy surfaces using neural networks and rotational spectra of the Ar–N_2 complex. *Mol. Phys.* **2016**, *114*, 72-82.

(36) Henderson, G.; Ewing, G. E. Infra-red spectrum, structure and properties of the N_2–Ar van der Waals molecule. *Mol. Phys.* **1974**, *27*, 903-915.

(37) McKellar, A.R.W. Infrared spectra of the $(N_2)_2$ and N_2–Ar van der Waals molecules. *J. Chem. Phys.* **1988**, *88*, 4190-4196.

(38) Jäger, W.; Gerry, M.C.L. The microwave spectrum of the van der Waals complex Ar-N_2. *Chem. Phys. Lett.* **1992**, *196*, 274-279.

(39) Jäger, W.; Gerry, M. C. L.; Bissonnette, C.; McCourt, F. R.W. Pure rotational spectrum of, and potential-energy surface for, the Ar–N_2 Van der Waals complex. *Faraday Discuss*. **1994**, *97*, 105-118.

(40) Hewage, J. W.; Amar, F. G. Structural motifs and stability of small argon–nitrogen clusters. *J. Chem. Phys.* **2003**, *119*, 9021-9029.

(41) Hewage, J. W.; Amar, F. G.; de Feraudy, M.-F.; Torchet, G. The structure of mixed nitrogen–Argon clusters. *Eur. Phys. J. D*. **2003**, *24*, 249-252.

(42) Torchet, G.; de Feraudy, M.-F.; Loreaux, Y. Electron diffraction studies on mixed Ar+N_2 clusters. *J. Mol. Struct.* **1999**, *261*, 485–486.

(43) Fort, E.; Pradère, F.; De Martino, A.; Vach, H.; Châtelet, M. Diagnostics of mixed van der Waals clusters. *Eur. Phys. J. D.* **1998**, *1*, 79-84.

(44) Rühl, E.; Hitchcock, A. P.; Morin, P.; Lavollée, M. Core excitation in atomic and molecular clusters. *J. Chem. Phys.* **1995**, *92*, 521-540.

(45) Yang, S.; Philippe, L.; Châtelet, M. Formation and Characterization of Large $(Ar)_n$, $(N_2)_n$, and Mixed $(Ar)_n(N_2)_m$ van der Waals Clusters Produced by Supersonic Expansion. *J. Clust. Sci.* **2007**, *18*, 855–867.

(46) Nagasaka, M.; Serdaroglu, E.; Flesch, R.; Rühl, E.; Kosugi, N. Structures of mixed argon-nitrogen clusters. *J. Chem. Phys.* **2012**, *137*, 214305.

(47) Sanaa Zaag, A.; Yazidi, O.; Jaidane, N.-E.; Ross, M. W.; CastlemanJr., A. W.; Al-Mogren, M. M.; Linguerri R.; Hochlaf, M. Structure, Reactivity, and Fragmentation of Small Multi-Charged Methane Clusters. *J. Phys. Chem. A*. **2016**, *120*, 1669-1676.

(48) Elstner, M.; Hobza, P.; Frauenheim, T.; Suhai, S.; Kaxiras, E. Hydrogen bonding and stacking interactions of nucleic acid base pairs: A density-functional-theory based treatment. *J. Chem. Phys.* **2001**, *114*, 5149-5155.

(49) Jurečka, P.; Černý, J.; Hobza, P.; Salahub, D. R. Density functional theory augmented with an empirical dispersion term. Interaction energies and geometries of 80 noncovalent complexes compared with *ab initio* quantum mechanics calculations. *J. Comput. Chem.* **2007**, *28*, 555-569.

(50) Boussouf, K.; Boulmene, R.; Prakash, M.; Komiha, N.; Taleb, M.; Al-Mogren M. M.; Hochlaf, M. Characterization of Zn^{q+} –imidazole (q = 0, 1, 2) organometallic complexes: DFT methods *vs.* standard and explicitly correlated post-Hartree–Fock methods. *Phys. Chem. Chem. Phys.* **2015**, *17*, 14417-14426.

(51) Boulmene, R.; Boussouf, K.; Prakash, M.; Komiha, N.; Al-Mogren M. M.; Hochlaf, M. Ab Initio and DFT Studies on CO_2 Interacting with Zn^{q+}–Imidazole (q=0, 1, 2) Complexes: Prediction of Charge Transfer through σ- or π-Type Models. *Phys. Chem. Chem. Phys.* **2016**, *17*, 994-1005.

(52) Mahjoubi, K.; Benoit, D. M.; Jaidane, N.-E.; Al-Mogren M. M.; Hochlaf, M. Understanding of matrix embedding: a theoretical spectroscopic study of CO interacting with Ar clusters, surfaces and matrices. *Phys. Chem. Chem. Phys.* **2015**, *17*, 17159-17168.

(53) VandeVondele, J.; Hutter, J. Gaussian basis sets for accurate calculations on molecular systems in gas and condensed phases. *J. Chem. Phys.* **2007**, *127*, 114105.

(54) Naumkin, F. Y.; Knowles, P. J. On the adequacy of pairwise additive potentials for rare gas–halogen systems: The effect of anisotropy of interactions between atoms. *J. chem. Phys.* **1995**, *103*, 3392-3399.

(55) Naumkin, F. Y.; Knowles, P. J.; *Femtochemistry - Ultrafast Chemical and Physical Processes in Molecular Systems*, edited by Chergui M. World Scientific :Singapore, **1996**, p.94.

(56) Goedecker, S.; Teter M.; Hutter, J. Separable dual-space Gaussian pseudopotentials. *Phys. Rev. B.* **1996**, *54*, 1703-1710.

(57) Lippert, G.; Hutter, J.; Parrinello, M. A hybrid Gaussian and plane wave density functional scheme. *Mol. Phys.* **1997**, *92*, 477-488.

(58) Krack, M.; Parrinello, M. in *High performance computing in chemistry, Report of the BMBF project, Grant Number 01IRA17 A-C*, edited by Grotendorst J.; FZ Jülich, Germany, **2004**, vol**.** 25 of NIC series.

(59) VandeVondele, J.; Krack, M.; Mohamed, F.; Parrinello, M.; Chassaing T.; Hutter, J. Quickstep: Fast and accurate density functional calculations using a mixed Gaussian and plane waves approach. *Computer Physics Communications*. **2005**, *167*, 103–128.

(60) Mundy, C. J.; Mohamed, F.; Schiffman, F.; Tabacchi, G.; Forbert, H.; Kuo, W.; Hutter, J.; Krack, M.; Iannuzzi, M.; McGrath, M. et al. CP2K software package, http://cp2k.berlios.de

(61) Krack, M. Pseudopotentials for H to Kr optimized for gradient-corrected exchange-correlation functional. *Theor. Chem. Acc.* **2005**, *114*, 145-152.

(62) Perdew, J. P.; Burke, K.; Ernzerhof, M. Generalized Gradient Approximation Made Simple. *Phys. Rev. Lett.* **1996**, *77*, 3865-3868.

(63) Byrd, R. H.; Lu, P.; Nocedal J.; Zhu, C. A Limited Memory Algorithm for Bound Constrained Optimization. *SIAM J. Sci. Comput.* **1995**, *16*, 1190-1208.

(64) Liu, B.; McLean, A. D. Accurate calculation of the attractive interaction of two ground state helium atoms. *J. Chem. Phys.* **1973**, *59*, 4557-4558.

(65) Knowles, P. J.; Andrews, J. S.; Amos, R. D.; Handy, N. C.; Pople, J. A. Restricted Møller—Plesset theory for open-shell molecules. *Chem. Phys. Lett.* **1991**, *186*,130-136.

(66) Møller C.; Plesset, M. S. Note on an Approximation Treatment for Many-Electron Systems. *Phys. Rev.* **1934**, *46*, 618-622.

(67) Curtiss, L. A.; Redfern, P. C.; Raghavachari, K.; Rassolov V.; Pople, J. A. Gaussian-3 theory using reduced Møller-Plesset order. *J. Chem. Phys.* **1999**, *110*, 4703-4709.

(68) Gaussian 09, Revision A.1, Frisch, M. J.; Trucks, G. W.; Schlegel, H. B.; Scuseria, G. E.; Robb, M. A.; Cheeseman, J. R.; Scalmani, G.; Barone, V.; Mennucci, B.; Petersson, G. A. et al. Gaussian, Inc., Wallingford CT, 2009.)

(69) **CFOUR, Coupled-Cluster techniques for Computational Chemistry**, a quantum-chemical program package by J.F. Stanton, J. Gauss, M.E. Harding, P.G. Szalay with contributions from A.A. Auer, R.J. Bartlett, U. Benedikt, C. Berger, D.E. Bernholdt, Y.J. Bomble, L. Cheng, O. Christiansen, F. Engel, R. Faber, M. Heckert, O. Heun, C. Huber, T.-C. Jagau, D. Jonsson, J. Jusélius, K. Klein, W.J. Lauderdale, F. Lipparini, D.A. Matthews, T. Metzroth, L.A. Mück, D.P. O'Neill, D.R. Price, E. Prochnow, C. Puzzarini, K. Ruud, F. Schiffmann, W. Schwalbach, C. Simmons, S. Stopkowicz, A. Tajti, J. Vázquez, F. Wang, J.D. Watts and the integral packages *MOLECULE* (J. Almlöf and P.R. Taylor), *PROPS* (P.R. Taylor), *ABACUS* (T. Helgaker, H.J. Aa. Jensen, P. Jørgensen, and J. Olsen), and ECP routines by A. V. Mitin and C. van Wüllen. For the current version, see http://www.cfour.de.

(70) Boys, S. F.; Bernardi, F. The calculation of small molecular interactions by the differences of separate total energies. Some procedures with reduced errors. *Mol. Phys.* **1970**, *19*, 553-566.

(71) K. P. Huber and G. Herzberg, Molecular Spectra and Molecular Structure IV, Constants of diatomic MoleculesNew York, Reinhold, 1979.

(72) Fujii, Y.; Lurie, N. A.; Pynn, R.; Shirane, G. Inelastic neutron scattering from solid ^{36}Ar. *Phys. Rev. B.* **1974**, *10*, 3647-3659.

(73) Halo, M.; Casassa, S.; Maschio, L.; Pisani, C. Local MP2 periodic study of rare-gas crystals. *Chem. Phys. Letters.* **2009**, *467*, 294–298.

(74) Prakash, M.; Mathivon, K.; Benoit, D. M.; Chambaud G.; Hochlaf, M. Carbon dioxide interaction with isolated imidazole or attached on gold clusters and surface: competition between σ H-bond and π stacking interaction. *Phys. Chem. Chem. Phys.* **2014**, *16*, 12503–12509.

(75) Iori, F.; Corni S.; Di Felice, R. Unraveling the Interaction between Histidine Side Chain and the Au(111) Surface: A DFT Study. *J. Phys. Chem. C.* **2008**, *112*, 13540–13545.

(76) Lowen, H. W.; Jodl, H. J.; Loewenschuss A.; Daufer, H. Raman studies on N_2 – rare-gas mixed crystals. *Can. J. Phys.* **1988**, *66*, 308-315.

(77) Anderson, D. T.; Davis S.; Nesbitt, D. J. Sequential solvation of HCl in argon: High resolution infrared spectroscopy of Ar_nHCl (n=1,2,3). *J. Chem. Phys.* **1997**, *107*, 1115-1127.

Graphical Abstract